Available online at www.sciencedirect.com
SCIENCE DIRECT®
Surface Science 588 (2005) L209–L219
SURFACE SCIENCE
www.elsevier.com/locate/susc

Surface Science Letters

Finite size effects on supported Pd nanoparticles: Interaction of hydrogen with CO and C_2H_4

Matthias Morkel, Günther Rupprechter *, Hans-Joachim Freund

Fritz-Haber-Institut der Max-Planck-Gesellschaft, Department of Chemical Physics, Faradayweg 4-6, D-14195 Berlin, Germany

Received 3 February 2005; accepted for publication 11 May 2005
Available online 16 June 2005

Abstract

Pd-hydride formation proceeds predominantly via minority sites on Pd nanoparticles (defects and (1 0 0) facets). Finite size effects govern the surface chemistry, e.g. "explosive" hydrogen desorption in the presence of a CO overlayer originates from the confinement of dissolved hydrogen within the limited nanoparticle volume. In situ surface vibrational spectra, acquired during CO hydrogenation under technical conditions, suggest surface roughening or a partly disordered CO adsorbate phase that only occur at elevated pressure. The presence of Pd-hydride phases yielded a very high activity for C_2H_4 hydrogenation on the Pd nanoparticles which may again be related to the hydrogen confinement effect.

Keywords: Sum frequency generation; Palladium; Clusters; Carbon monoxide; Hydrogen molecule; Alkenes; Low-index single crystal surfaces; Catalysis; Vibrations of adsorbed molecules

1. Introduction

A knowledge of the morphology of supported metal nanoparticles is of tremendous importance in heterogeneous catalysis because the catalytic properties of nanoparticles strongly depend on their exact surface structure ([1–9] and references therein). Metal nanoparticles often exhibit low Miller-index facets and single crystal surfaces have therefore frequently been used as model systems. Provided that the support material is rather inert, the catalytic properties of a low-index plane on metal nanoparticles and of the corresponding single crystal surface should be similar (at least for particles larger than 2–3 nm).

Combining non-linear optical sum frequency generation (SFG) vibrational spectroscopy and thermal desorption spectroscopy (TDS) we demonstrate that this assumption of similar properties is not necessarily justified. For the interaction of

* Corresponding author. Fax: +49 30 8413 4105.
E-mail address: rupprechter@fhi-berlin.mpg.de (G. Rupprechter).

0039-6028/$ - see front matter © 2005 Elsevier B.V. All rights reserved.
doi:10.1016/j.susc.2005.05.037

CO and H_2 pronounced differences exist between well-faceted Pd nanoparticles and Pd(1 1 1). In this letter, we focus on the properties of Pd nanoparticles while experiments on Pd(1 1 1) were described in detail previously [10]. The Pd nanoparticles were supported by a thin Al_2O_3 film [8] grown on a NiAl(1 1 0) substrate and had the shape of truncated cuboctahedra, as revealed by scanning tunneling microscopy (STM) (mean diameter: ~6 nm; height: ~2 nm; ~3000 atoms/particle; ~600 surface atoms/particle; $\sim 1 \times 10^{12}$ particles/cm^2; cf. Fig. 1) [8,11]. Although ~80% of the surface of the Pd nanoparticles consisted of (1 1 1) facets (with the remaining ~20% being (1 0 0) facets), their properties were markedly different from Pd(1 1 1).

We examine dissociative hydrogen adsorption and dissolution and CO–H coadsorption, which is an elementary step of catalytic CO hydrogenation [12]. Hydrogen dissolution and hydride formation were facilitated for Pd nanoparticles, which also influenced CO–H coadsorption. Of course, one could argue that Pd nanoparticles could be better modeled by other (stepped/kinked) single crystal surfaces. However, we show that the desorption of dissolved hydrogen was governed by the limited volume (or *finite size*) of Pd nanoparticles and not by their specific surface structure. Apparently, a volume on the nm^3 scale cannot be modeled by macroscopic single crystals. SFG spectroscopy allowed us to obtain vibrational spectra of adsorbed molecules under ultrahigh vacuum (UHV) as well as at "high-pressure" (mbar to 1 bar) [9,13,14]. In situ SFG spectra illustrate that the dynamic equilibrium adsorbate structure present during a high-pressure/high-temperature CO hydrogenation reaction was different from that observed under static UHV conditions. To further exploit the effect of Pd-hydrides, SFG and TDS studies of C_2H_4–H interaction were performed which indicate that Pd-hydrides may also influence the reactivity of Pd nanoparticles for olefin hydrogenation.

2. Experimental

Experiments were performed in a UHV system combined with an SFG-compatible UHV-high-pressure cell [9,15]. Pd–Al_2O_3/NiAl(1 1 0) model

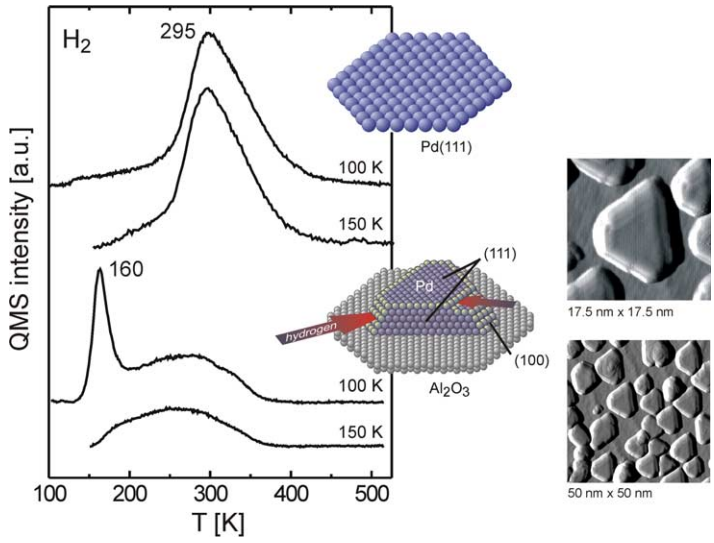

Fig. 1. Thermal desorption spectra of hydrogen acquired after H_2-exposure to Pd–Al_2O_3 and Pd(1 1 1): cooling in 2×10^{-7} mbar H_2 from 300 K to 100 K (~80 L; upper traces) and cooling in 2×10^{-7} mbar H_2 from 300 K to 150 K (~150 L; lower traces). Schematic models and STM images of the Pd model catalysts are shown on the right. For simplicity, the ball model shows a smaller particle but with the correct proportions.

catalysts were prepared by growing a thin ordered Al_2O_3 film (thickness ~0.5 nm) on NiAl(1 1 0) by two cycles of oxidation in 10^{-6} mbar O_2 at 523 K, followed by Pd (purity ⩾ 99.99%) electron beam evaporation at 300 K [8,16] and a "stabilization" treatment as described in [17]. The reproducibility of the Pd nanoparticle preparation was confirmed by sample transfer to an STM (using a vacuum-suitcase) and by electron microscopy inspection of the samples [16]. Pd(1 1 1) was prepared by standard procedures [15].

For a description of SFG theory and the laser setup we refer to [9,15]. Briefly, picosecond laser pulses at a tunable infrared frequency ω_{IR} and at a fixed visible frequency ω_{vis} are spatially and temporally overlapped on the sample surface. When the IR frequency coincides with an adsorbate vibrational resonance, a sum frequency signal ($\omega_{SFG} = \omega_{IR} + \omega_{vis}$) is generated. Plotting the SFG signal vs. the IR wavenumber yields a vibrational spectrum. Since SFG is only allowed in a medium without inversion symmetry, the signal is generated by the adsorbate/Pd interface, while the isotropic gas phase gives no signal. TPD spectra were recorded with a heating rate of 1 K/s with CO coverages being determined by integration of TPD areas, with the (2×2) 0.75 ML CO saturation structure on Pd(1 1 1) serving as reference. To avoid "non-equilibrium" CO structures [18] some exposures were carried out by "downcooling" the Pd samples in the respective gas.

To remove Ni- and Fe-carbonyl impurities, CO (purity ⩾ 99.997%) was passed over a carbonyl absorber cartridge and then introduced via a cold trap filled with liquid nitrogen. Hydrogen (purity ⩾ 99.99990) and ethylene (purity ⩾ 99.95) were cleaned using a cold trap. For UHV exposures the pressure indicated by the ionization gauge was corrected by the sensitivity factors for CO (1.0), H_2 (0.44) and C_2H_4 (~2). When gas mixtures were used, CO and H_2 were premixed in a glass bulb at mbar pressures using a baratron gauge.

3. Results and discussion

In this section hydrogen adsorption and hydride formation will be presented first, followed by CO–H coadsorption under UHV and by CO–H interaction at elevated (mbar) pressure. To examine the possible influence of Pd-hydrides on molecules other than CO, results on C_2H_4 hydrogenation are finally discussed.

3.1. Hydrogen adsorption and Pd-hydride formation

Fig. 1 compares H_2–TDS spectra of Pd–Al_2O_3 and Pd(1 1 1). Here we distinguish adsorbed surface hydrogen, subsurface hydrogen (which is not necessarily restricted to in between the first and second substrate layers but may be situated within the first 5–10 layers below the surface [19–21]; this species is sometimes called "near-surface hydrogen" or "near-surface hydride"), and bulk hydrogen dissolved deep below the surface. It is interesting to note that subsurface and bulk hydrogen were previously suggested to exhibit higher catalytic activity than adsorbed hydrogen [22–24].

On Pd(1 1 1), exposure to H_2 during cooling from 300 K to 100 K (~80 L) led to a desorption peak at 295 K, due to recombinative hydrogen desorption from surface sites (with possible small contributions of subsurface and bulk hydrogen). In contrast, for Pd–Al_2O_3 a sharp desorption peak appeared at 160 K, followed by a broad desorption up to ~350 K.[1] While the latter mostly originates from surface H, the 160 K peak indicates subsurface hydrogen. Assuming that the broad peak around 250 K corresponds to a hydrogen coverage (θ) of 1 ML, the average particle composition is $PdH_{0.3}$ (including subsurface and surface H). When more H_2 was exposed to the Pd particles (~5500 L at 120 K) the 160 K peak increased and the amount of subsurface hydrogen exceeded that of surface hydrogen by three times (stoichiometry of ~$PdH_{0.8}$). Therefore, we attribute the 160 K peak (which is reminiscent of a so-called "hydrogen explosion" [25]) to the decomposition of a Pd-hydride. Here "Pd-hydride" includes solid solutions as well as hydride phases with varying stoichiometry and structure.

[1] Nearly identical spectra were obtained by dosing 20–50 L hydrogen at 120 K.

A "near-surface hydride" similar to the one in Fig. 1 was previously reported for Pd(1 1 1) but its formation required much higher exposures (~5000 L at 115 K) [21]. An easier hydride formation was reported for more open surfaces, e.g. (below 140 K) ~300 L are sufficient on Pd(1 0 0) [26], ~50 L on Pd(1 1 0) [27], ~200 L on Pd(3 3 1) [28] and ~40 L on Pd(2 1 0) [19]. This indicates that the activation barriers for H *surface to subsurface* diffusion on more open surfaces are smaller than on Pd(1 1 1). Consequently, since hydride formation is strongly facilitated for Pd particles (as compared to Pd(1 1 1)) it must proceed predominantly via the small (1 0 0) facets and defects. Apparently, "minority sites" (on (1 0 0) facets (<20%) and/or edges/steps/defects (<10%)) rather than the more abundant (1 1 1) facets govern the hydrogen absorption properties of Pd nanoparticles. The picture of hydrogen surface to subsurface diffusion via defects is corroborated by observations that after roughening Pd(1 1 1) by ion bombardment or on (presumably rough) Pd films hydride formation increased [21,29].

After H_2 exposure during cooling from 300 K to 150 K (~150 L), the 160 K peak was not observed (Fig. 1) because the near-surface hydride is not stable at 150 K. Nevertheless, the onset of hydrogen desorption was still ~70 K lower for Pd–Al_2O_3 than for Pd(1 1 1), presumably due to the small particle volume (an influence of defects can, however, currently not be excluded) [24]. When the temperature is increased during TPD, on Pd(1 1 1) H has the additional option to diffuse deeper in the bulk [10,15] while for nanoparticles H is restricted to their small volume providing a reservoir which can supply H rapidly to the surface. As shown below, this effect has a strong impact on CO–H coadsorption and cannot be mimicked by macroscopic single crystals.

3.2. CO–H coadsorption under UHV

Fig. 2 shows a coadsorption experiment under UHV, dosing H_2 first and CO second. After saturation with hydrogen, H_2–TDS traces as described above were observed (cf. Figs. 1 and 2b and d). No SFG signals (apart from the non-resonant background; dashed lines) were detected because the Pd–H stretch (~500 cm^{-1}) is too low for our setup. The small peak in CO–TDS (Fig. 2b and d) indicates a negligible amount of residual CO [15]. After dosing CO on the H-covered surfaces at 150 K, SFG indicated adsorbed CO on Pd(1 1 1) and Pd–Al_2O_3 (Fig. 2a and c). The different lineshape of the SFG spectra for Pd particles originates from the NiAl(1 1 0) substrate which increases the non-resonant background and changes its phase difference to the resonant signal (this has no influence on the adsorbate). The SFG spectra were fitted according to Eqs. (1) and (2) in [16] (red lines)[2] and the resonance frequency and linewidth are indicated. On Pd(1 1 1), SFG detected bridge (1966 cm^{-1}) and on-top (2090 cm^{-1}) bonded CO ($\theta \sim 0.65$ ML). On Pd nanoparticles the SFG spectra were dominated by a peak at 1990 cm^{-1}, with additional weaker signals at 2100, ~1965 cm^{-1} and ~1865 cm^{-1} (typical of a near saturation coverage). The intense peak at ~1990 cm^{-1} originates from CO on (1 0 0) facets [30] and from CO bridge bonded to particle edges and steps [16,31]. However, in light of the particle shape the (1 0 0) facets and the particle edges are "minority sites" (~20% and <10% of the surface atoms, respectively) which cannot explain the large intensity of the 1990 cm^{-1} peak. "Intensity borrowing" from bridging CO on (1 1 1) facets (~1965 cm^{-1}) may therefore enhance the 1990 cm^{-1} peak [8,30,32]. The peaks at 2100 cm^{-1} and ~1865 cm^{-1} are due to on-top and hollow CO on (1 1 1) facets, respectively.

The amount of adsorbed CO can be deduced from CO–TDS (Fig. 2b and d). The TDS spectra were identical to those after dosing the same CO amount at 150 K on the clean samples, demonstrating that the surfaces were fully covered with CO and that H was replaced from the Pd surface. However, H had not desorbed as H_2–TDS (Fig. 2b and d) indicated that the hydrogen amount was unchanged. Apparently, CO had displaced surface H to the subsurface and bulk of Pd(1 1 1) and of the Pd nanoparticles (partial H spillover to the

[2] For interpretation of color in Figs. 2, 3 and 5, the reader is referred to the web version of the article.

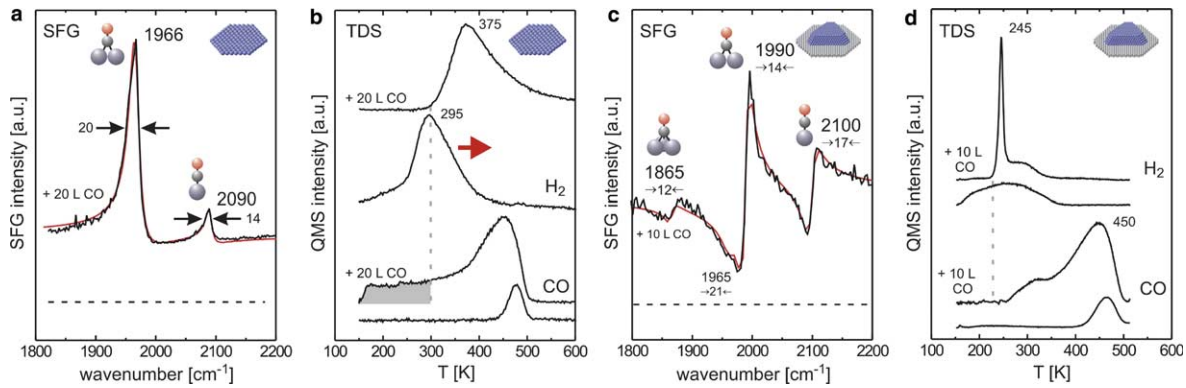

Fig. 2. Sequential dosing of H_2 and CO on Pd–Al_2O_3 and Pd(1 1 1): After cooling in 2×10^{-7} mbar H_2 from 300 K to 150 K (~150 L), SFG (a, c), and TDS (b, d) measurements were taken (lower traces). After repeating the H_2 exposure and subsequently adsorbing 10–20 L CO at 150 K, SFG and TDS spectra were again acquired (a–d; upper traces).

support is unlikely because no OH groups or H_2O were detected).

With respect to the *desorption* of dissolved hydrogen there are striking differences between Pd particles and Pd(1 1 1). Approx. 50% of the hydrogen desorbs from the particles in a very sharp peak (Fig. 2d), similar to the decomposition of the Pd-hydride phase in Fig. 1. This indicates that CO had displaced H to the subsurface of the nanoparticles, increasing the near-surface H concentration and producing a hydride-like phase even at 150 K. Resulting from the CO overlayer on the Pd particles the hydrogen desorption maximum shifted to 245 K but desorption still occurred *before* CO desorption started. For Pd(1 1 1), the replacement of surface H by CO did not produce such a sharp H_2 desorption peak (Fig. 2b) and H_2 desorption started only *after* a considerable amount of CO had desorbed, generating free sites for H recombination (shaded area in Fig. 2b; H_2 desorption starts after the CO coverage has become lower than 0.55 ML and the desorption maximum was at 0.33 ML CO). Apart from the differences between Pd–Al_2O_3 and Pd(1 1 1) discussed above, the "explosive" desorption of the hydride phase "through" a CO-layer which *only occurs for Pd nanoparticles* is remarkable.

At first, one may expect that *structural effects* are responsible. However, we found that it is rather the finite particle size that is important. When hydride decomposition generates a hydrogen "pressure" inside a Pd nanoparticle the small volume does not allow to accommodate excess hydrogen. Thus, surface CO is pushed aside enabling hydrogen desorption "through" the CO overlayer. In contrast, when CO prevents H_2 desorption on Pd(1 1 1), near-surface hydrogen has the *additional* option to diffuse deeper into the bulk during the TPD run (which leads to high temperature tailing in Fig. 2b) [20,21,26,27].

To experimentally differentiate *structure and volume* effects, Pd(1 1 1) and Pd(1 1 0) crystals were exposed to large amounts of hydrogen (ca. 10.000 L at 130 K) to produce near-surface hydrides [21,27], followed by 20 L CO to replace surface hydrogen. In subsequent TDS experiments, hydrogen desorption started only above 300 K (maximum ~370 K; similar to Fig. 2b), including a high temperature tail. Similar results were reported for Pd(1 1 0) and Pd(1 0 0) [27,33]. Consequently, for Pd(1 1 1), (1 1 0) and (1 0 0) single crystals it seems to be easier to decompose a near-surface hydride by H bulk dissolution than by replacing surface CO and subsequent desorption. Such a route is not feasible on nanoparticles which suggests that the observed hydrogen desorption in the presence of a CO layer is in fact *related to the limited volume of the Pd nanoparticles* and not to their particular surface structure. A contribution from desorption via the metal–oxide interface can, however, currently not be excluded.

When the experiment of Fig. 2 was carried out at 100 K, the result was qualitatively the same for Pd nanoparticles while CO was unable to adsorb on H-precovered Pd(1 1 1). At 100 K, the barriers for H surface to subsurface diffusion cannot be easily overcome on Pd(1 1 1) (~0.5 eV [10]) and H can hence not be displaced by CO [15]. Coadsorption experiments with 1:1 CO/H_2 mixtures at 100 K were again qualitatively the same for Pd nanoparticles, while on-top CO was "destabilized" on Pd(1 1 1) (H atoms diffusing between hollow sites via bridge sites shift on-top CO to bridge sites; for details see [10]). Both effects are again related to the higher H surface to subsurface diffusion barrier on Pd(1 1 1) and will be presented in detail elsewhere.

Under the conditions of TPD coadsorption experiments no reaction products of CO hydrogenation were detected, most likely due to the small reaction probability (and for Pd(1 1 1) further complicated by H dissolution leading to a (partial) separation of H (in the bulk) and surface CO). In order to try to stimulate a CO–H reaction at high temperature, SFG experiments were carried out at elevated pressure, as described in the next section.

3.3. CO–H interaction at atmospheric pressure

We have also acquired SFG spectra under high-pressure/high-temperature conditions, similar to those of heterogeneous catalysis [12,34,35] when a dynamic equilibrium between gas phase and surface species is established (Fig. 3). Of course, in "real" systems the CO/H_2 pressure (10–25 bar) is still higher but increasing the pressure by up to six orders of magnitude induced only small changes in CO coverage (Fig. 3). At 500 K the CO frequency is red-shifted due to a reduction in coverage and there is also a temperature-induced line broadening [30]. In any case, the SFG spectrum at 1.1 bar on Pd–Al_2O_3 (Fig. 3b) is very similar to IR spectra reported by Hicks and Bell [34] for 5% Pd–SiO_2 at ~10 bar, indicating that our model catalysts mimics a technical catalyst quite well.

SFG indicated high CO coverages (~0.5 ML on Pd(1 1 1) and close to saturation on Pd particles). Under static UHV conditions, such high CO coverages prevent dissociative hydrogen adsorption [15], in accordance with the ~2.5 eV activation barrier suggested by DFT for hydrogen adsorption on CO-covered Pd(1 1 1) [10]. Furthermore, recent STM observations of H/Pd(1 1 1) suggest that dissociative hydrogen adsorption requires at least three neighboring empty Pd sites [36] which are difficult to find at such high CO coverages and render hydrogen adsorption even more unlikely. However, a static (UHV) picture is not appropriate here. Under the dynamic conditions of a high-pressure reaction even the unlikely event of hydrogen adsorption has a non-zero probability due the adsorption/desorption equilibrium of CO and the high hydrogen impingement rate (which is about 40 times higher than that of CO and on the order of 10^8/Pd surface atom/sec). Isotope exchange experiments indicated that even at 200 K a CO layer was exchanged within minutes [16]. Even if only a negligible number of free adsorption sites is present resulting from thermal fluctuations on the CO covered surface (e.g. one site per 10^6 Pd atoms), the high H_2 impingement rate allows for a non-negligible hydrogen adsorption. At high gas temperatures, the increased fraction of high kinetic energy hydrogen molecules may also raise the reaction probability.

Under the high-pressure/high-temperature conditions we have also observed another effect that may facilitate the reaction between CO and hydrogen (apart from the high impingement rates). The high-pressure spectra in Fig. 3a and b were different from corresponding UHV spectra for θ_{CO} ~0.5. On Pd(1 1 1) at 500 K, a peak at 1925 cm^{-1} was accompanied by weak features at ~2025 cm^{-1} and ~2070 cm^{-1}, the latter two pointing to on-top CO (Fig. 3a). It should be noted that for low temperature (UHV) CO spectra a bridge (or hollow) bonded CO signal around 1925 cm^{-1} *did not occur* in combination with on-top CO [15,16].[3] Consequently, the species at 2070 cm^{-1}

[3] At half monolayer coverage CO produces a c(4 × 2) overlayer on Pd(1 1 1), consisting of two different domains, i.e. one with CO in fcc and hcp threefold hollow sites and one with bridge bonded CO [15]. Since vibrational spectroscopy only detects a single peak at 1920 cm^{-1} we do not differentiate between hollow and bridge bonded CO.

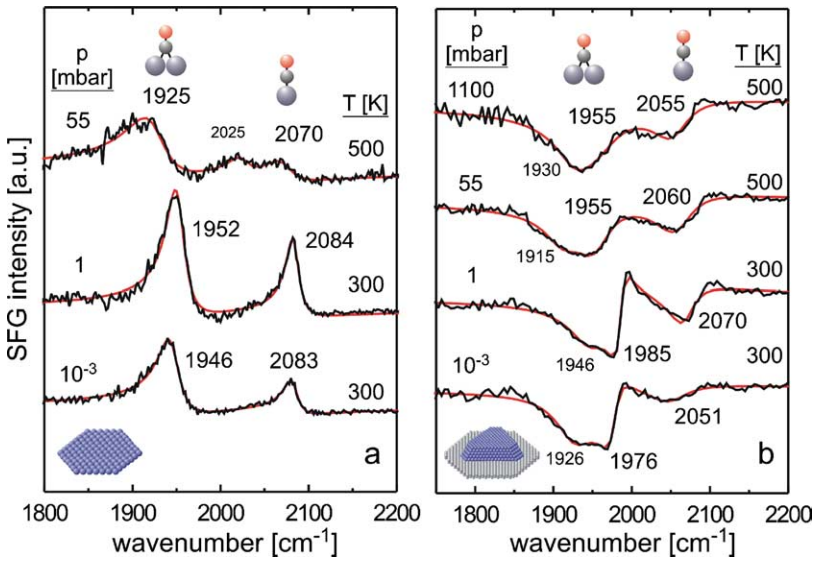

Fig. 3. High-pressure SFG spectra of a 1:10 CO/H_2 mixture on Pd(1 1 1) (a) and on Pd–Al_2O_3 (b). Pressures and temperatures are indicated.

and 2025 cm^{-1} may indicate that the Pd(1 1 1) surface is (partially) roughened under reaction conditions (particularly the low-frequency on-top CO species should originate from CO bonded to low-coordinated sites) [37]. A (compared to UHV spectra) modified adsorbate structure was also observed for Pd–Al_2O_3 where a bridging species at 1955 cm^{-1} was accompanied by an on-top feature around 2060 cm^{-1} (Fig. 3b). Such a low-frequency on-top CO species does not occur under UHV [38] and again points to a possible surface roughening. However, the high-pressure adsorbate phase was not induced by hydrogen because corresponding spectra of (pure) CO were nearly identical. In any case, post-reaction CO-SFG did not indicate any surface reconstruction or modified spectrum demonstrating that the CO-induced roughening must be either reversible or rather moderate, if present at all.

Alternatively, the additional on-top CO species at mbar pressure can also originate from a not perfectly ordered CO phase which may facilitate CO–H interaction. Taking into account DFT calculations favoring the CO + H reaction over a single metal atom [39] the on-top CO species would react with hollow bonded H to produce CHO (formyl). Although further experiments and calculations are required to understand this adsorbate structure, it is evident that the equilibrium conditions of a high-pressure reaction led to adsorbate arrangements that could not be reproduced under static UHV conditions.

With respect to the catalytic activity at ambient conditions we have tried to detect reaction products (methanol or methane) by gas chromatographic (GC) and mass spectroscopic (MS) detection but only trace amounts of products were found. This is due to the small turnover frequency of Pd ($\sim 5 \times 10^{-4}\ s^{-1}$ at 550 K) [35,40] and the small Pd surface area of our catalysts (~0.25–0.5 cm^{-2}) yielding product quantities below the GC detection level. The high CO coverage under reaction conditions certainly contributes to the low CO hydrogenation rate. However, in light of the good resemblance between our SFG spectra and those of Hicks and Bell on technical catalyst the SFG spectra are certainly characteristic for the adsorbate geometry under reaction conditions (but we have to refer to [34] for a description of kinetic data).

Surface H diffuses easily into the Pd bulk under reaction conditions and large amounts of H_2 were actually detected by post-reaction H_2–TDS. Although β-Pd-hydride is not stable under the

applied reaction conditions (H_2 pressure up to 1 bar, temperature up to 550 K), there is a considerable amount of dissolved hydrogen and its involvement in the catalytic reaction cannot be ruled out. In fact, the selectivity of Pd(1 1 1) for hydrodechlorination was shown to be different for adsorbed and "bulk hydrogen" [23].

3.4. C_2H_4 hydrogenation

In order to address the specific activity of Pd-hydride phases and their interaction with other molecules than CO we have studied the coadsorption and reaction of C_2H_4 and H on Pd nanoparticles and Pd(1 1 1). Fig. 4 compares TDS traces of H_2 (mass 2), C_2H_4 (monitored by mass 27), and C_2H_6 (monitored by mass 29) measured after adsorption of the individual components (Fig. 4a and b) as well as after H–C_2H_4 coadsorption (Fig. 4c). SFG signals of C_2H_4 adsorbed on Pd particles turned out to be too weak for detection but SFG spectra on Pd(1 1 1) are shown in Fig. 5 for reference (for TDS measurements on Pd(1 1 1) see [10,41,42]).

Adsorbing 50 L H_2 on well-facetted Pd nanoparticles at 120 K produced a TDS pattern typical of adsorbed H and Pd-hydride (Fig. 4a), as described above (C_2H_4 and C_2H_6 desorption traces are also displayed to exclude the adsorption of residual gases). After adsorbing 1.5 L C_2H_4 on well-facetted Pd nanoparticles at 120 K (Fig. 4b), C_2H_4–TDS revealed a broader peak with a maximum at 265 K and a small desorption feature at 185 K. The TDS trace is quite similar to that on Pd(1 1 1) [10] indicating that the spectrum is dominated by desorption from the (1 1 1) particle facets (C_2H_4 desorption from Pd(1 0 0) is not too different, though [43]). SFG of C_2H_4 on Pd(1 1 1) indicated bands at 2910 cm^{-1} and 2960 cm^{-1} (Fig. 5a; the latter can be discerned by fitting), characteristic of $\nu_S(CH_2)$ vibrations of di-σ- and π-bonded ethylene, respectively [44]. The weak SFG signal of π-bonded ethylene originates from the orientation of the C–H bonds nearly parallel to the metal surface [45] and possibly also from its small surface concentration.

Taking into account these spectra and IRAS spectra on Pd nanoparticles ([46,47] and references therein) the 265 K peak can be attributed to di-σ-bonded ethylene while the 185 K feature is most likely due to π-bonded ethylene or to rearrangements in the ethylene layer upon desorption [10]. This agrees with theoretical studies suggesting a combination of di-σ-bonded C_2H_4 at bridge sites and π-bonded C_2H_4 at on-top sites as surface species at low adsorption temperature [45,48]. Some

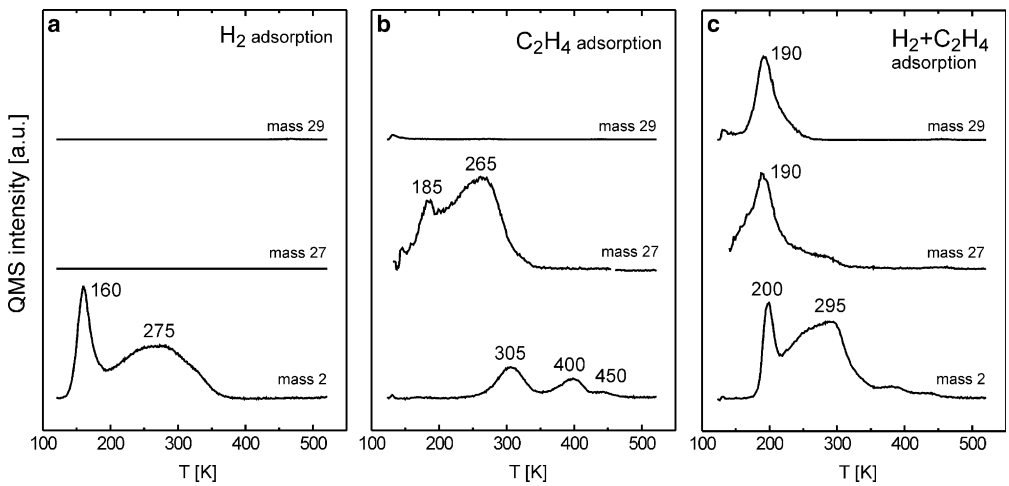

Fig. 4. Thermal desorption spectra of H_2 (mass 2), C_2H_4 (monitored by mass 27), and C_2H_6 (monitored by mass 29) measured after adsorption of H_2 (a), C_2H_4 (b), and after H–C_2H_4 coadsorption (c). Exposures were 50 L H_2 at 120 K (a), 1.5 L C_2H_4 at 120 K (b) and 50 L H_2 followed by 1.5 L C_2H_4 at 120 K (c).

ethylene decomposes into ethylidyne C_2H_3 around 300 K (characteristic $\nu_S(CH_3)$ at 2870 cm^{-1}; Fig. 5c) which further dehydrogenates at higher temperature, explaining the H_2 desorption in Fig. 4b [44,49–52].

For the H–C_2H_4 coadsorption experiment (Fig. 4c), 50 L hydrogen were adsorbed on Pd–Al_2O_3 at 120 K, immediately followed by 1.5 L C_2H_4 (preadsorbed C_2H_4 would prevent H adsorption). As evident from SFG (Fig. 5b; and IRAS [42,53]) and from TDS (Fig. 4c) C_2H_4 was now mostly bonded in a π-configuration while the amount of di-σ-bonded ethylene was reduced. This can be understood by considering that preadsorbed H occupies threefold hollow sites and influences the adsorption of di-σ-bonded ethylene (at bridge sites [45,48]) while π-bonded C_2H_4 can still adsorb on-top of Pd atoms. The change in the C_2H_4 adsorption configuration may indicate the coexistence of C_2H_4 and H on the surface at 120 K but electronic effects of subsurface H should also be considered as possible explanation [54] (e.g. H could be replaced from the surface by C_2H_4).

The most striking result of the H–C_2H_4 coadsorption experiment (Fig. 4c) is related to the H_2 and C_2H_6 desorption. The H_2-desorption peak attributed to the decomposition of Pd-hydride was shifted from 160 to 200 K. This is less than the corresponding shift for H–CO coadsorption (85 K; cf. Fig. 2d) but still reveals an effect of the C_2H_4 overlayer on H_2-desorption (either by stabilizing the hydride or, more likely, by hindering hydrogen recombination). Most interestingly, C_2H_6 was produced and desorbed around 190 K with a C_2H_6 TDS-desorption signal (monitored by mass 29) *nearly as intense* as that of C_2H_4 (monitored by mass 27) (Fig. 4c). This is remarkable because previous H–C_2H_4 coadsorption TDS studies, carried out *in the absence of distinct hydride phases*, had reported a C_2H_6 desorption signal that was typically much smaller than that of C_2H_4 (on the order of a few percent) on Pd–Al_2O_3 [24,41] and even less on Pd(1 1 1) [41,42].[4] The much higher C_2H_6 formation of Fig. 4c thus suggests a direct involvement of Pd-hydride in the hydrogenation reaction.

To deduce an *inherently* higher catalytic activity of dissolved hydrogen (Pd-hydrides or subsurface H) from these measurements is, however, not unambiguous. One has to consider that the apparently higher concentration of surface hydrogen at the reaction temperature around 190 K (due to the decomposition of the Pd-hydride phase supplying H to the surface) may simply cause the high C_2H_4 conversion. As discussed in more detail in [10], the low C_2H_4 hydrogenation activity of Pd(1 1 1) in TDS can be rationalized by considering that surface H (partly) dissolves in the Pd bulk during TDS (at ~125–200 K) which leads to a depletion of surface H (decreasing the reaction probability). When H "returns" to the surface (and desorbs in the range 250–400 K), C_2H_4 has already mostly desorbed. This explanation is also supported by the observation that TDS detects the maximum of C_2H_6 formation/desorption on

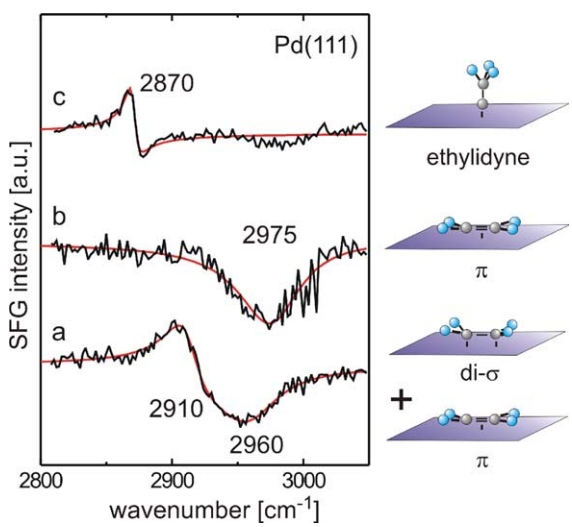

Fig. 5. SFG spectra of C_2H_4 species on Pd(1 1 1). Exposures were 2.5 L C_2H_4 at 100 K (a), 1 L H_2 followed by 2.5 L C_2H_4 at 100 K (b). Spectrum (c) was acquired at 300 K after annealing in 5×10^{-7} mbar C_2H_4 from 100 to 300 K.

[4] TDS studies of C_2H_4 hydrogenation [41,42] typically monitor mass 30 or 29 for C_2H_6 and mass 28, 27 or 26 for C_2H_4. Variations in the masses used (e.g. 30/28 vs. 29/27) induce only minor sensitivity changes that are much smaller than the effect reported here. Nevertheless, in light of experimental differences, we did not attempt a quantitative analysis. Cracking pattern for C_2H_6 (mass/percent) 30/28%, 29/23%, 28/100%, 27/35%, 26/24%; for C_2H_4 (mass/percent) 28/100%, 27/63%, 26/54%.

Pd(1 1 1) around 270 K [41,42], i.e. ~80 K higher than on Pd particles. For Pd nanoparticles, even in the absence of hydride phases, the overall availability of hydrogen is higher because hydrogen dissolution is restricted to the small volume of a Pd nanoparticle.

When C_2H_4 hydrogenation was carried out at atmospheric pressure (50 mbar C_2H_4, 200 mbar H_2, 750 mbar He, 300 K) the specific activity per Pd surface atom was very similar for Pd nanoparticles and Pd(1 1 1) (turnover frequency ~5 site^{-1} sec^{-1}) [55–57]. Under these conditions, Pd-hydrides are certainly present (beside adsorbed H) but their inherently higher activity can still not be proven. In situ SFG spectra of C_2H_4 hydrogenation at mbar pressure did not reveal any surface species, pointing to a low adsorbate/intermediate concentration under reaction conditions.

4. Conclusions

Combined SFG/TDS measurements have revealed distinct differences in H adsorption/dissolution and CO–H coadsorption between supported Pd nanoparticles and Pd(1 1 1) even though the particle surface is dominated by (1 1 1) facets. Minority species such as (1 0 0) facets and edge and defect sites govern the properties of the nanoparticles for the processes examined. A hydride phase was more easily formed on Pd nanoparticles due to lower activation barriers for H surface to subsurface diffusion. The confinement of dissolved H within the limited volume of a Pd nanoparticle is responsible for differences in the desorption of dissolved hydrogen from clean and CO-covered Pd–Al_2O_3 and Pd(1 1 1). In the presence of Pd-hydride a very high activity for C_2H_4 hydrogenation was observed. However, since the decomposition of Pd-hydride also increases the concentration of surface H, an inherently higher activity of dissolved hydrogen can currently not be proven. SFG spectra acquired under the equilibrium conditions of a high-pressure high-temperature CO hydrogenation reaction were different from those obtained under static UHV conditions. At mbar pressure, dissociative hydrogen adsorption may occur despite the high CO coverage and may be facilitated by surface roughening or a partly disordered CO phase that are only present under reaction conditions.

Acknowledgements

We acknowledge support by Priority Program SPP 1091 of the German Science Foundation (project Ru 831/1-4). We also thank M. Heemeier and M. Bäumer for the STM images in Fig. 1.

References

[1] R. van Hardeveld, A. van Montfoort, Surf. Sci. 4 (1966) 396.
[2] M. Che, C.O. Bennet, Adv. Catal. 36 (1989) 55.
[3] A.K. Datye, D.J. Smith, Catal. Rev.—Sci. Eng. 34 (1992) 129.
[4] G. Rupprechter, K. Hayek, L. Rendón, M. José-Yacamán, Thin Solid Films 260 (1995) 148.
[5] M. Bäumer, L. Libuda, A. Sandell, H.-J. Freund, G. Graw, T. Bertrams, H. Neddermeyer, Ber. Bunsenges. Phys. Chem. 99 (1995) 1381.
[6] H.-J. Freund, Angew. Chem. Int. Ed. Engl. 36 (1997) 452.
[7] C.R. Henry, Surf. Sci. Rep. 31 (1998) 235.
[8] H.-J. Freund, M. Bäumer, H. Kuhlenbeck, Adv. Catal. 45 (2000) 412.
[9] G. Rupprechter, Phys. Chem. Chem. Phys. 3 (2001) 4621.
[10] G. Rupprechter, M. Morkel, H.-J. Freund, R. Hirschl, Surf. Sci. 554 (2004) 43.
[11] K.H. Hansen, T. Worren, S. Stempel, E. Lægsgaard, M. Bäumer, H.-J. Freund, F. Besenbacher, I. Stensgaard, Phys. Rev. Lett. 83 (1999) 4120.
[12] C. Chinchen, P.J. Denny, J.R. Jennings, M.S. Spencer, K.C. Waugh, Appl. Catal. 36 (1988) 1.
[13] G.A. Somorjai, G. Rupprechter, J. Phys. Chem. B 103 (1999) 1623.
[14] G. Rupprechter, H.-J. Freund, Top. Catal. 14 (2001) 3.
[15] M. Morkel, G. Rupprechter, H.-J. Freund, J. Chem. Phys. 119 (2003) 10853.
[16] H. Unterhalt, G. Rupprechter, H.-J. Freund, J. Phys. Chem. B 106 (2002) 356.
[17] S. Shaikhutdinov, M. Heemeier, J. Hoffmann, I. Meusel, B. Richter, M. Bäumer, H. Kuhlenbeck, J. Libuda, H.-J. Freund, R. Oldman, S.D. Jackson, C. Konvicka, M. Schmid, P. Varga, Surf. Sci. 501 (2002) 270.
[18] M. Morkel, H. Unterhalt, M. Salmeron, G. Rupprechter, H.-J. Freund, Surf. Sci. 532–535 (2003) 103.
[19] U. Muschiol, P.K. Schmidt, K. Christmann, Surf. Sci. 395 (1998) 182.
[20] M. Wilde, M. Matsumoto, K. Fukutani, T. Aruga, Surf. Sci. 482 (2001) 346.

[21] G.E. Gdowski, T.E. Felter, R.H. Stulen, Surf. Sci. 181 (1987) L147.
[22] S.P. Daley, A.L. Utz, T.R. Trautman, S.T. Ceyer, J. Am. Chem. Soc. 116 (1994) 6001.
[23] G. Rupprechter, G.A. Somorjai, Catal. Lett. 48 (1997) 17.
[24] A. Doyle, S. Shaikhutdinov, S.D. Jackson, H.-J. Freund, Angew. Chem. Int. Ed. Engl. 42 (2003) 5240.
[25] K. Christmann, F. Chehab, V. Penka, G. Ertl, Surf. Sci. 152/153 (1985) 356.
[26] H. Okuyama, W. Siga, N. Takagi, M. Nishijima, T. Aruga, Surf. Sci. 401 (1998) 344.
[27] R.J. Behm, V. Penka, M.-G. Cattania, K. Christmann, G. Ertl, J. Chem. Phys. 78 (1983) 7486.
[28] D. Farias, P. Schilbe, M. Patting, K.H. Rieder, J. Chem. Phys. 110 (1999) 559.
[29] H. Cordatos, T. Bunluesin, R.J. Gorte, Surf. Sci. 323 (1995) 219.
[30] F.M. Hoffmann, Surf. Sci. Rep. 3 (1983) 103.
[31] I.V. Yudanov, R. Sahnoun, K.M. Neyman, N. Rösch, J. Hoffmann, S. Schauermann, V. Johánek, H. Unterhalt, G. Rupprechter, L. Libuda, H.-J. Freund, J. Phys. Chem. B 107 (2003) 255.
[32] P. Hollins, Surf. Sci. Rep. 16 (1992) 51.
[33] C. Nyberg, L. Westerlund, Surf. Sci. 256 (1991) 9.
[34] R.F. Hicks, A.T. Bell, J. Catal. 90 (1984) 205.
[35] A.F. Gusovius, T.C. Watling, R. Prins, Appl. Catal. A 188 (1999) 187.
[36] T. Mitsui, M.K. Rose, E. Fomin, D.F. Ogletree, M. Salmeron, Nature 422 (2003) 705.
[37] R.K. Brandt, R.S. Sorbello, R.G. Greenler, Surf. Sci. 271 (1992) 605.
[38] K. Wolter, O. Seiferth, H. Kuhlenbeck, M. Bäumer, H.-J. Freund, Surf. Sci. 399 (1998) 190.
[39] M. Neurock, Top. Catal. 9 (1999) 135.
[40] P.J. Berlowitz, D.W. Goodman, J. Catal. 108 (1987) 364.
[41] A. Doyle, S. Shaikhutdinov, H.-J. Freund, J. Catal. 223 (2004) 444.
[42] D. Stacchiola, S. Azad, L. Burkholder, W.T. Tysoe, J. Phys. Chem. B 105 (2001) 11233.
[43] E.M. Stuve, R.J. Madix, J. Phys. Chem. 89 (1985) 105.
[44] M. Kaltchev, A.W. Thompson, W.T. Tysoe, Surf. Sci. 391 (1997) 145.
[45] Q. Ge, M. Neurock, Chem. Phys. Lett. 358 (2002) 377.
[46] M. Frank, M. Bäumer, Phys. Chem. Chem. Phys. 2 (2000) 3723.
[47] M. Frank, M. Bäumer, R. Kühnemuth, H.-J. Freund, J. Vac. Sci. Technol. A 19 (2001) 1497.
[48] M. Neurock, R.A. van Santen, J. Phys. Chem. B 104 (2000) 11127.
[49] S. Shaikhutdinov, M. Heemeier, M. Bäumer, T. Lear, D. Lennon, R.J. Oldman, S.D. Jackson, H.-J. Freund, J. Catal. 200 (2001) 330.
[50] M. Sock, A. Eichler, S. Surnev, J.N. Andersen, B. Klötzer, K. Hayek, M.G. Ramsey, F.P. Netzer, Surf. Sci. 545 (2003) 122.
[51] D. Stacchiola, G. Kaltchev, G. Wu, W.T. Tysoe, Surf. Sci. 470 (2000) L32.
[52] L.L. Kesmodel, J.A. Gates, Surf. Sci. 111 (1981) L747.
[53] D. Stacchiola, L. Burkholder, W.T. Tysoe, Surf. Sci. 511 (2002) 215.
[54] D. Stacchiola, W.T. Tysoe, Surf. Sci. 540 (2003) L600.
[55] G. Rupprechter, H. Unterhalt, M. Morkel, P. Galletto, L. Hu, H.-J. Freund, Surf. Sci. 502–503 (2002) 109.
[56] H.-J. Freund, M. Bäumer, J. Libuda, T. Risse, G. Rupprechter, S. Shaikhutdinov, J. Catal. 216 (2003) 223.
[57] G. Rupprechter, Annu. Rep. Prog. Chem. C 100 (2004) 237.